JOURNAL OF VISUAL COMMUNICATION AND IMAGE REPRESENTATION
Vol. 9, No. 4, December, pp. 392–400, 1998
ARTICLE NO. VC980394

A Power Differentiation Method of Fractal Dimension Estimation for 2-D Signals

P. Asvestas, G. K. Matsopoulos, and K. S. Nikita

Department of Electrical and Computer Engineering, National Technical University of Athens, Athens, Greece

Received February 16, 1998; accepted August 7, 1998

Fractal dimension has been used for texture analysis as it is highly correlated with the human perception of surface roughness. Several methods have been proposed for the estimation of the fractal dimension of an image. One of the most popular is via its power spectrum density, provided that it is modeled as a fractional Brownian function. In this paper, a new method, called the power differentiation method (PDM), for estimating the fractal dimension of a two-variable signal from its power spectrum density is presented. The method is first applied to noise-free data of known fractal dimension. It is also tested with noise-corrupted and quantized data. Particularly, in the case of noise-corrupted data, the modified power differentiation method (MPDM) is developed, resulting in more accurate estimation of the fractal dimension. The results obtained by the PDM and the MPDM are compared directly to those obtained using four other well-known methods of fractal dimension. Finally, preliminary results for the classification of ultrasonic liver images, obtained by applying the new method, are presented. © 1998 Academic Press

1. INTRODUCTION

Fractal geometry was introduced and developed by Mandelbrot [1] as a means for describing and analyzing the properties of objects with irregular and complex structure (fractals), such as coastlines and surfaces of mountains. The characteristic property of a fractal is that it is self-similar for every scale of analysis. This fact implies that any part of a fractal object is a scaled-down copy of the original. However, for natural objects the self-similarity is observed only for a limited range of scales and it appears in a statistical sense. In this case, a part of the object, magnified to the size of the original, exhibits statistical properties similar to those of the original. The numerical quantification of self-similarity is obtained by the fractal dimension.

The fractal dimension is a measure of the roughness of the surface represented by the fractal set: the larger the fractal dimension is, the rougher the surface appears. This fact has led to the utilization of the fractal dimension and other fractal-based features as descriptors of the texture of images [2–6]. Applications of the fractal theory in image analysis also include image segmentation [2, 6–8], shape description [9], object characterization [10], and surface reconstruction [11], while there are several nice results on the fractal dimension estimator using wavelets [12]. The fractal model has been used in medical imaging for analysis of bone X-rays [13, 14], classification of ultrasonic liver images [15], edge enhancement [15, 16], and mammogram analysis [17].

In this paper, a new method, called the power differentiation method (PDM), for estimating the fractal dimension of a two-variable signal from its power spectrum density is presented. Along with the PDM a robust fitting technique for obtaining the fractal dimension from the resulting log–log plot is described. The method is first applied to noise-free data of known fractal dimension. Then it is tested with noise-corrupted data and quantized data (gray-level images). Particularly, in the case of noise-corrupted data, a modification of the method, called the modified power differentiation method (MPDM), is proposed, resulting in more accurate estimation of the fractal dimension. Results obtained by the PDM and the MPDM are compared directly to results obtained using four other well-known methods of fractal dimension estimation. Finally, preliminary results for the classification of ultrasonic liver images, obtained by applying the new method, are presented.

2. FRACTAL DIMENSION: DEFINITION AND ESTIMATION METHODS

There are several definitions of the fractal dimension, FD, of a set. The most popular of them is the box-counting dimension, which is an upper limit of the Hausdorff–Besicovich dimension [1]. The box-counting dimension of a set $S \subset R^n$ is defined as

$$\mathrm{FD} = \lim_{r \to 0} \frac{\log N(r)}{\log(1/r)}, \qquad (1)$$

1047-3203/98 $25.00

where $N(r)$ denotes the number of n-dimensional cubes, size r, needed to cover set S.

The methods for the estimation of the fractal dimension of an image, $I(m, n)$, of size $M \times N$ can be grouped into three categories; fractional Brownian motion (fBm) methods, area measurement methods, and box-counting methods. The main representatives from each category are the following.

2.1. *Power Spectrum Method* (*PSM*)

This method belongs to the fractional Brownian motion (fBm) methods. The image is assumed to be fBm [2, 18, 19] with parameter

$$H = 3 - \mathrm{FD} \tag{2}$$

with $0 < H < 1$.

Then the power spectrum density of image is given by

$$P(f_1, f_2) = \frac{k}{(\sqrt{f_1^2 + f_2^2})^b} = \frac{k}{f^b}, \tag{3}$$

where k is a positive constant. The exponent b is related to the fractal dimension as

$$b = 2 + 2H = 2(4 - \mathrm{FD}), \tag{4}$$

where $2 \leq b \leq 4$.

Equation (3) actually describes an average power spectrum density [20], since for fBm processes, due to their nonstationarity [20], the power spectrum density cannot be derived by the Fourier transform of the autocorrelation function.

Pentland [2] estimated the exponent b for various directions of the Fourier plane as the slope of the least-squares line at the points ($-\log f$, $\log P(f_1, f_2)$). These estimates were then collapsed into one average measurement, from which the fractal dimension was obtained.

2.2. *Difference Statistics Method* (*DSM*)

This method also belongs to the fBm methods, where the following relation is assumed to hold [2],

$$E[|\Delta I_\Delta|] = E[|\Delta I_{\Delta r = l}|](\Delta r)^H, \tag{5}$$

where $\Delta I_{\Delta r} = I(m + \Delta m, n + \Delta n) - I(m, n)$ with $\Delta r = \sqrt{(\Delta m)^2 + (\Delta n)^2}$, c is a constant, and $E[\cdot]$ denotes the expectation value. Then the H parameter is estimated by the slope of the line that fits best at the points ($\log \Delta r$, $\log E[|\Delta I_{\Delta r}|]$).

2.3. *Covering Blanket Method* (*CBM*)

This method belongs to the area measurement methods. The area of the image intensity surface at scale ε is given by the relation

$$A(\varepsilon) = C\varepsilon^{2-\mathrm{FD}},$$

where C is a constant. Peleg [3] suggested that the area $A(\varepsilon)$ be estimated ($\varepsilon = 1, 2, \ldots,$) by the relation

$$A(\varepsilon) = \frac{V(\varepsilon) - V(\varepsilon - 1)}{2},$$

where $V(\varepsilon)$ is the volume of the blanket, of thickness 2ε, covering the image intensity surface. The fractal dimension is obtained as 2-s, where s is the slope of the best fitting line at the points ($\log \varepsilon$, $\log A(\varepsilon)$).

2.4. *Box Counting Method* (*BCM*)

In the box-counting method, the estimation of the fractal dimension is based on Eq. (1). The image plane (m, n) is covered by a 3-dimensional grid of cubes for various grid sizes r. The number of cubes, $N(r)$, containing at least one pixel of the image is counted and the fractal dimension is obtained by the slope of the best fitting line at the points ($-\log r$, $\log N(r)$). Modifications of the box-counting method can be found in [21].

3. POWER DIFFERENTIATION METHOD (PDM)

In this section, a new method, called the Power Differentiation Method (PDM), for estimating the fractal dimension of a two variable fBm function, $B_{\mathrm{H}}(x_1, x_2)$, from its average power spectrum is presented.

According to Eq. (3), the average power spectrum density of $B_{\mathrm{H}}(x_1, x_2)$ is given by

$$P(f_1, f_2) = \frac{k}{(\sqrt{f_1^2 + f_e^2})^\beta}.$$

Let $I(f_r)$ denote the power of the signal for the bandwidth of radial frequencies $[f_0, f_r]$:

$$\begin{aligned} I(f_r) &= \iint_{f_0 \leq \|\mathbf{f}\| \leq f_r} P(f_1, f_2)\, df_1\, df_2 \\ &= \iint_{f_0 \leq \|\mathbf{f}\| \leq f_r} \frac{k}{(\sqrt{f_2^2 + f_2^2})^\beta}\, df_1\, df_2. \end{aligned}$$

By changing the Cartesian coordinates (f_1, f_2) to the polar (f, φ), where $f = \sqrt{f_1^2 + f_2^2}$ and $\varphi = \tan^{-1}(f_1, f_2)$, we obtain

$$I(f_r) = k \int_0^{2\pi} d\varphi \int_{f_0}^{f_r} f^{1-b}\, df = \frac{2\pi k}{2-b}\left(\frac{1}{f_r^{b-2}} - \frac{1}{f_0^{b-2}}\right).$$

The derivative, $I'(f_r)$, of $I(f_r)$ with respect to f_r is given by the relation

$$I'(f_r) = \frac{dI}{df_r} = \frac{2\pi k}{f_r^{b-1}}.$$

Thus, $b - 1$ is the slope of the straight line described by the equation

$$\log I'(f_r) = \log(2\pi k) + (b-1)(-\log f_r). \tag{6}$$

Consequently, the fractal dimension is obtained using Eqs. (6) and (4).

It is very important to note that the presence of additive noise does not degrade the robustness of the estimator. Actually, in the presence of white, additive noise, which happens quite often, the proposed method gives a more robust estimate of the fractal dimension than using Eq. (3) directly, as the PSM does. It is not difficult to show that in the presence of white noise with power spectrum density equal to N_0, the expression for the derivative of the power, $I_n'(f_r)$, of the noise-corrupted signal can be written in the following form

$$I_n'(f_r) = 2\pi\left(\frac{k}{f_r^{b-1}} + N_0\right),$$

while Eq. (3) is modified as follows:

$$P_n(f_r) = \frac{k}{f_r^b} + N_0.$$

Recalling that $b > 2$ and noticing that $\frac{1}{f_r^{b-1}} > \frac{1}{f_r^b}$ for $f_r > 1$, we conclude that the signal component in the expression for $I_n'(f_r)$ is greater than that in the expression for $P_n(f_r)$. This means that, in the presence of white noise, the useful component in the two expressions is higher in the PDM, which can result in more accurate estimates of the fractal dimension.

In practice, discrete data $B_H(m_1T_s, m_2T_s)$, with $m_1 = 0, 1, \ldots, M_1 - 1$, $m_2 = 0, 1, \ldots, M_2 - 1$, and $T_s = 1/f_s$ the sampling period, are available. The average power spectrum density, $P(F_1, F_2)$, for the normalized pair of frequencies (F_1, F_2), with $F_1 = f_1/f_s = n_1/M_1$, $F_2 = f_2/f_s = n_2/M_2$ ($n_1 = 0, 1, \ldots, M_1 - 1$, $n_2 = 0, 1, \ldots, M_2 - 1$) is approximated by $P(F_1, F_2) = |K(F_1, F_2)|^2$, where

$$K(F_1, F_2) = \sum_{m_1=0}^{M_1-1}\sum_{m_2=0}^{M_2-1} B_H(m_1T_s, m_2T_s)\exp[-2\pi j(m_1F_1 + m_2F_2)]$$

is the discrete 2-D Fourier transform of $B_H(m_1T_s, m_2T_s)$.

The power $I(F_r)$, for various normalized radial frequencies, $F_r = f_r/f_s$, is approximated by the double sum

$$I(F_r) \approx \sum_{F_1}\sum_{F_2} P(F_1, F_2),$$

where $F_0 \le \sqrt{F_1^2 + F_2^2} \le F_r$ and $F_0 = f_0/f_s$.

The derivative $I'(F_r)$ is then estimated using the Savitzky–Golay smoothing filter [22]. For a given data set $\{z_i\}$ ($i = 1, 2, \ldots, N$), the Savitzky–Golay smoothed first derivative, at position j, is estimated by the derivative, at the same position, of the least-squares fit polynomial (usually of order 4 or higher) at the points $\{z_{j-m_w}, \ldots, z_j, \ldots, z_{j+n_w}\}$, where n_w and n_w are positive integers.

Ideally, according to Eq. (6), all points ($-\log F_r$, $\log I'(F_r)$) must lie on a straight line, namely $-d \log I'(F_r)/d \log(F_r) = b - 1$, for every F_r. In the practice, the discrete nature of the procedure for calculating $I'(F_r)$, as well as the fact that Eq. (3) does not hold for every value of f for real data, cause the points ($-\log F_r$, $\log I'(F_r)$) not to lie exactly on a straight line. Therefore, $b - 1$ is estimated usually by the slope of the best-fitting line at the points ($-\log F_r$, $\log I'(F_r)$), using the least-squares method.

For a set of data points (x_i, y_i), $i = 1, 2, \ldots, N$, the parameters of the best-fitting line, in the least-squares sense, $y = p + qx$, are obtained by minimizing, with respect to p and q, the function

$$h_{\mathrm{LSq}}(p, q) = \sum_{i=1}^{N} d_i^2 = \sum_{i=1}^{N}(y_i - p - qx_i)^2.$$

However, the least-squares fitting is not a robust method; points deviating much from the straight line, called outliers, can cause the resulting line to be a very bad fit. A more robust method can be obtained if the function to be minimized is chosen in such a way that the outliers influence the fit less. Such a robust method is the M-estimation method [22], where the function to be minimized is

$$h_{\mathrm{MEst}}(p, q) = \sum_{i=1}^{N} \rho(d_i^2), \tag{7}$$

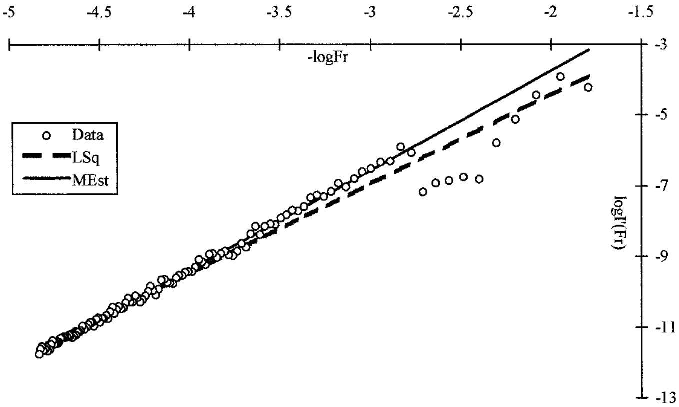

FIG. 1. Fitting a straight line at the data points ($-\log F_r$, $\log I'(F_r)$) by the least-squares method and the M-estimation method.

where ρ is a symmetric, positive valued function with a unique minimum at zero; for example, such a function is $\rho(x) = \log(1 + x^2/2)$.

In order to demonstrate the superiority of the robust fitting method against the least-squares method, the two methods were applied to a set of points ($-\log F_r, \log I'(F_r)$) obtained by a 256×256 data set with true fractal dimension 2.1. The results are shown in Fig. 1, where it can be observed that the M-estimation method in contrast to the least-squares method, ignores the outliers, resulting in a more accurate estimation of the fractal dimension. Indeed, the estimated values were $FD_{LSq} = 2.240$ for the least-squares method and $FD_{MEst} = 2.093$ for the M-estimation method. Actually the fluctuations at lower frequencies as displayed in Fig. 1 were generated artificially, adding uniformly distributed random numbers to $\log I'(F_r)$, and they did not arise from the application of the estimator to the data set. The reason for this was to emphasize the superiority of the robust fitting against the least-squares method.

4. MODIFIED POWER DIFFERENTIATION METHOD (MPDM)

The presence of white noise causes the flattening of the average power spectrum density, particularly for high radial frequencies, which in turn causes the deformation of the scatter plot $\log I'(F_r)$ vs $-\log(F_r)$, as shown in Fig. 2. Thus, there is a (normalized) radial frequency, $F_{r,\max}$, depending on the level of the noise, which is the upper limit of the range of the frequencies over which the fitting procedure must be done. This critical frequency can be estimated as follows.

Due to the fact that $B_H(m_1T_s, m_2T_s)$ is a discrete fBm function, its 2-D discrete Fourier transform is given by

$$K(F_1, F_2) = \frac{\alpha(F_1, F_2)}{(\sqrt{F_1^2 + F_2^2})^b} e^{j\varphi(F_1,F_2)} = \frac{\alpha(F_1, F_2)}{F^{b/2}} e^{j\varphi(F_1,F_2)},$$

where $F = \sqrt{F_1^2 + F_2^2}$ is the normalized radial frequency, $\alpha(F_1, F_2)$ is a Rayleigh distributed random variable such that $E[\alpha^2(F_1, F_2)] = A_2$ and $\varphi(F_1, F_2)$ is uniform in $[0, 2\pi)$.

If $n(m_1T_s, m_2T_s)$ denotes a sample from zero-mean, white, noise random process with standard deviation σ, then its 2-D discrete Fourier transform is

$$N(F_1, F_2) = n(F_1, F_2) e^{j\theta(F_1,F_2)}$$

where $n(F_1, F_2)$ is a Rayleigh distributed random variable such that $E[n^2(F_1, F_2)] = \sigma^2$ and $\theta(F_1, F_2)$ is uniform in $[0, 2\pi)$.

Thus, the 2-D discrete Fourier tranform of the function $g(m_1T_s, m_2T_s) = B_H(m_1T_2, m_2T_s) + n(m_1T_s, m_2T_s)$, is

$$G(F_1, F_2) = K(F_1, F_2) + N(F_1, F_2).$$

Thus, the average spectrum density of $g(m_1T_s, m_2T_s)$ is given by the relation

$$P_g(F_1, F_2) = E[|G(F_1, F_2)|^2] = \frac{A^2}{F^b} + \sigma^2.$$

Requiring

$$\frac{A^2}{F^b} \gg \sigma^2 \tag{8}$$

for every $F \leq F_{r,\max}$ results in $P_g(F_1, F_2) \approx A^2/F^b$.

Equation (8) is rewritten as

$$\frac{\sigma^2 F^b}{A^2} \ll 1$$

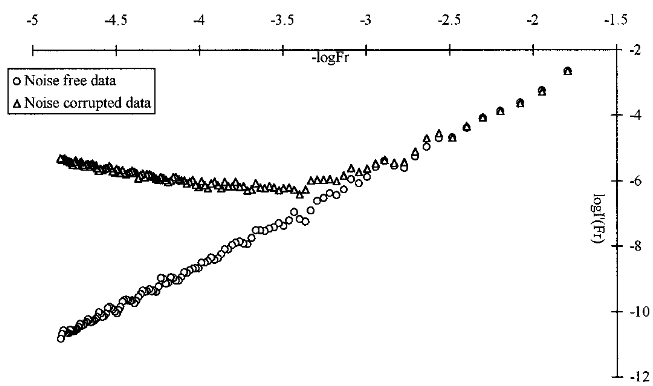

FIG. 2. Scatter plot of $\log I'(F_r)$ vs $-\log F_r$ for noise free data and corrupted data with white noise.

TABLE 1
Estimation of the Fractal Dimension of the Data Generated by the Fourier Filtering Method Applying the Five Methods

	PDM		PSM		DSM		CBM		RDBCM	
True	Mean	St.D.	Mean	St.D.	Mean	St.D.	Mean	St.D.	Mean	St.D.
2.2	2.206	0.025	2.207	0.072	2.297	0.045	2.266	0.046	2.104	0.031
2.4	2.403	0.026	2.412	0.076	2.423	0.044	2.392	0.043	2.197	0.029
2.6	2.609	0.028	2.585	0.070	2.558	0.040	2.526	0.046	2.295	0.031
2.8	2.802	0.026	2.794	0.083	2.691	0.029	2.670	0.038	2.393	0.022

or equivalently

$$\frac{\sigma^2 F^{\mathrm{b}}}{A^2} = c, \tag{9}$$

where $0 < c \ll 1$.

If $F_{r,\max}$ is chosen equal to

$$F_{r,\max} = \left(\frac{cA^2}{\sigma^2}\right)^{1/b}, \tag{10}$$

then indeed the relation (8) holds.

The MPDM for the estimation of the fractal dimension of corrupted data with white noise of known variance is based on a two-pass procedure. Firstly, an estimation of the parameters A and b is obtained for a small number of radial frequencies. Based on these estimates, the $F_{r,\max}$ is calculated from Eq. (10) for a very small value of c, for example $c = 10^{-5}$. Then the method is applied again for radial frequencies smaller than $F_{r,\max}$ and the final estimate of b is obtained. It must be noticed that this two-pass procedure can be applied to any other method of estimation of the fractal dimension based on the average power spectrum density.

5. EXPERIMENTAL RESULTS

5.1. Noise-Free Data

Five methods, including the PDM, were chosen for a comparative study. The other four methods were the power spectrum method (PSM) due to Pentland, the difference statistics method (DSM), the covering blanket method (CBM) and the relative differential box counting method (RDBCM) [21]. These methods were tested on data with known fractal dimension, generated by the Fourier filtering method [19]. Specifically, one hundred (100) two-dimensional fBm signals of size 128×128 were generated for each value of FD = 2.2, 2.4, 2.6, 2.8. The results of the estimations can be seen in Table 1, where the true fractal dimension, the mean and the standard deviation of the estimates are listed. The results in Table 1 suggest that the proposed method has the best performance amongst the methods in terms of accuracy and standard deviation of the estimates. The PSM performs equally well, the RDBCM underestimates the true value of fractal dimension, whereas the DSM and CBM seem to underestimate the true value only for high fractal dimensions (FD = 2.8).

The five method were also tested to another set of images generated by the random midpoint displacement method [19], which approximates the statistical model given by Eq. (5). The obtained estimates are listed in Table 2. The results indicate that the DSM yields reliable estimates for the full range of variation of the fractal dimension. The CBM gives very good estimates only when the true value of the fractal dimension is relatively low. The proposed method, for this set of data, provides reliable estimates for high values of the fractal dimension (for 2.6 or higher), whereas the PSM cannot give reliable estimates at all. Finally, the RDBCM underestimates the true value of fractal dimension.

It is important to note that the performance of any algo-

TABLE 2
Estimation of the Fractal Dimension of the Data Generated by the Random Midpoint Displacement Method Applying the Five Methods

	PDM		PSM		DSM		CBM		RDBCM	
True	Mean	St.D.	Mean	St.D.	Mean	St.D.	Mean	St.D.	Mean	St.D.
2.2	2.534	0.043	2.895	0.144	2.317	0.057	2.290	0.050	2.054	0.035
2.4	2.570	0.040	2.891	0.125	2.473	0.049	2.412	0.042	2.163	0.034
2.6	2.690	0.059	2.888	0.120	2.632	0.036	2.530	0.028	2.277	0.027
2.8	2.879	0.077	2.933	0.078	2.768	0.025	2.627	0.022	2.375	0.019

rithm derived for the estimation of the fractal dimension changes depending on the approximate fBm technique used for the generation of the data [23]. Therefore, for the first set of data, where Eq. (3) is used, the results are biased towards the PDM and the PSM, while for the second set, the results are biased towards the DSM. A more fair performance comparison would include the use fBm generation techniques not related to any of the estimators under study. Such a method, which generates true 2-D discrete fBm samples, is the Cholesky decomposition. However, the computational cost of the technique is too high [23].

5.2. Noise-Corrupted Data

The five methods were also tested on noise-corrupted data. White, Gaussian, zero mean noise was added to the data generated by the Fourier filtering method, for signal to noise ratio 10, 20, and 30 dB, where SNR $= 10 \log_{10} (P_s/\sigma^2)$, $P_s = 1/N^2 \sum_{i=1}^{N} \sum_{j=1}^{N} I(i, j)^2$ is the power of signal $I(i, j)$, and σ^2 is the variance of the noise. First, the PDM and the MPDM were tested on the noise corrupted data. The results obtained by the two methods are shown in Fig. 3.

From Fig. 3, it can be noticed that the performance of the PDM is affected deeply by the presence of noise, resulting in large deviation of the estimated fractal dimension from the true value. This is particularly true when the true fractal dimension is low (for example, FD = 2.2), even for moderate signal to noise ratio (for example SNR = 20 dB). On the other hand, the MPDM performs very well even for small SNR and for low fractal dimension. It must be noted that the same remarks hold also for other methods based on average power spectrum (PSM).

Next, the MPDM and the other four methods (PSM was also modified) were applied to the previous noise-corrupted data. The obtained results for FD = 2.2, 2.4, 2.6, and 2.8 are presented in Table 3. The results suggest that:

1. For SNR 30 dB, the MPDM ranks the best in terms of accuracy among the five methods, except for FD = 2.2, where the PSM gives a better estimate. The CBM and the DSM perform well, mainly, for FD = 2.4, 2.6, whereas the RDBCM clearly underestimates the true value, although the standard deviation of its estimates are the lowest.

2. For SNR 20 dB, the PSM, followed by the MPDM, has the best performance, regarding the accuracy, while the same remarks for SNR 30 dB hold for the CBM, DSM, and RDBCM.

3. For SNR 10 dB, the MPDM and the PSM perform the best in terms of accuracy. The DSM and CBM perform well only when the true value of the fractal dimension is relatively high (FD = 2.8), while the RDBCM seems to overestimate the true value for FD = 2.2 and underestimate for FD = 2.6, 2.8.

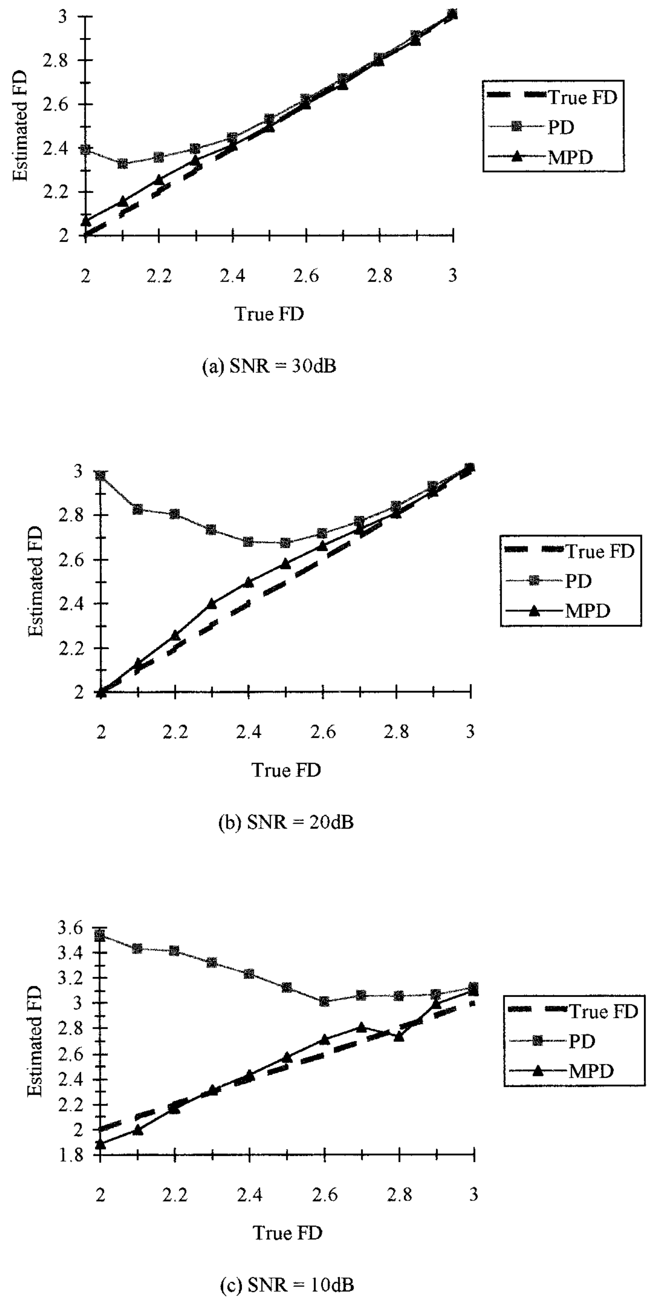

FIG. 3. Comparison of PDM and MPDM for noise corrupted data. (a) SNR 10 dB, (b) SNR 20 dB, and (c) SNR 10 dB.

5.3. Quantized Data

In order to examine the influence of the quantization on the estimation of the fractal dimension, the noise-free data previously generated by the Fourier filtering method were converted to gray images with 256 gray levels. The results obtained by the application of the five methods to the quantized data are shown in Table 4. Comparing Table 1 and Table 4, it follows that the

TABLE 3
Estimation of the Fractal Dimension of the Noise-Corrupted Data by the Five Methods

	MPDM		PSM		DSM		CBM		RDBCM	
	Mean	St.D.	Mean	St.D.	Mean	St.D.	Mean	St.D.	Mean	St.D.
					SNR = 30 dB					
2.2	2.255	0.067	2.245	0.155	2.315	0.039	2.282	0.040	2.116	0.027
2.4	2.414	0.033	2.442	0.120	2.431	0.042	2.398	0.040	2.202	0.027
2.6	2.600	0.032	2.607	0.098	2.561	0.039	2.529	0.045	2.298	0.031
2.8	2.796	0.082	2.826	0.086	2.692	0.029	2.671	0.037	2.395	0.022
					SNR = 20 dB					
2.2	2.259	0.161	2.234	0.249	2.413	0.024	2.374	0.022	2.191	0.019
2.4	2.497	0.117	2.413	0.191	2.482	0.030	2.446	0.028	2.240	0.021
2.6	2.664	0.055	2.609	0.160	2.584	0.032	2.552	0.039	2.315	0.024
2.8	2.810	0.087	2.834	0.122	2.702	0.027	2.680	0.036	2.402	0.020
					SNR = 10 dB					
2.2	2.171	0.293	2.199	0.424	2.682	0.040	2.645	0.040	2.414	0.039
2.4	2.433	0.183	2.457	0.307	2.680	0.026	2.643	0.026	2.399	0.024
2.6	2.718	0.128	2.589	0.246	2.710	0.020	2.679	0.023	2.415	0.018
2.8	2.740	0.223	2.823	0.240	2.766	0.017	2.748	0.026	2.454	0.014

quantization of the data affects minimally the performance of the five methods. The PDM method continues to perform the best amongst the methods regarding the accuracy and the standard deviation of the estimates. The RDBCM continues to underestimate the true value of the fractal dimension.

6. CLASSIFICATION OF ULTRASONIC LIVER IMAGES—PRELIMINARY RESULTS

The proposed method (PDM) was tested on a set of 21 ultrasonic liver images, comprising seven (7) images of normal liver and fourteen (14) images of abnormal liver (hepatoma: 7 images and hemangeoma: 7 images). The fractal dimension was estimated for each image using a 64 $\times$ 64 pixel block (region of interest-ROI). ROIs were chosen so that they were located as close to the center as possible, approximately at one of the transmit focal points and included solely liver parenchyma without including major blood vessels (Fig. 4). The results of the estimations as well as the mean and the standard deviation of the estimates are listed in Table 5.

From Table 5, it follows that the fractal dimension for the images of normal livers is below 2.9, whereas for the images of abnormal livers is above 2.9 (except for image Hem3). A fuzzy *c*-mean clustering algorithm [24] was applied for the classification of the images, based on the estimated fractal dimension, in two classes; normal and abnormal. Livers N1, N2, N3, N4, N5, N6, N7, and Hem 3 were classified as normal (class center = 2.629) and the rest as abnormal (class center = 3.169), which means that the correct classification percentage was 95.2%. The above results suggest that the fractal dimension, estimated by the proposed method, can be used as a feature for the discrimination between normal and abnormal livers. Similar results were obtained by Chen *et al.* [15] using a normalized fBm feature vector.

The above procedure was repeated using the DSM. The mean value and the standard deviation of the fractal dimension for normal and abnormal livers were 2.990 $\pm$

TABLE 4
Estimation of the Fractal Dimension of the Quantized Data by the Five Methods

	PDM		PSM		DSM		CBM		RDBCM	
True	Mean	St.D.	Mean	St.D.	Mean	St.D.	Mean	St.D.	Mean	St.D.
2.2	2.213	0.025	2.258	0.066	2.297	0.045	2.266	0.046	2.099	0.027
2.4	2.405	0.026	2.440	0.074	2.424	0.044	2.392	0.043	2.181	0.027
2.6	2.609	0.028	2.599	0.069	2.558	0.040	2.526	0.046	2.271	0.030
2.8	2.803	0.026	2.804	0.081	2.691	0.029	2.670	0.038	2.366	0.022

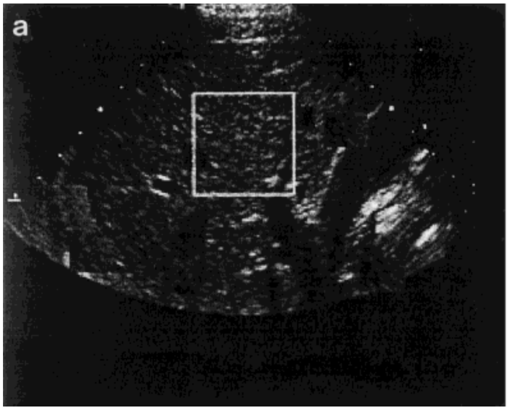

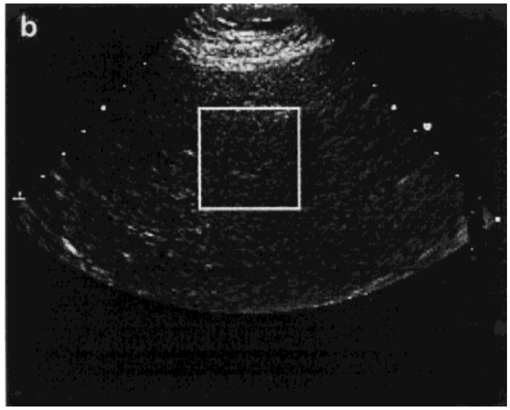

FIG. 4. Images from normal liver (a) and abnormal liver (b). The rectangular area in each image is the region of interest (ROI), whose size is 64 × 64 and from which the fractal dimension was estimated using the PDM.

0.019 and 2.944 ± 0.022, respectively. The percentage of correct classification was 85.7%, which means that 18 out of 21 images were correctly classified. The misclassifications occurred for images Hep4, Hep5, and N1.

7. CONCLUSIONS

In this paper, a new method, the power differentation method (PDM), for the estimation of the fractal dimension of a two-variable fBm function from its average power spectrum density was presented. A robust procedure was used for the fitting of a straight line at the points ($-\log F_r$, $\log I'(F_r)$). The PDM was applied to noise-free data and the results obtained were compared with those from four other well-known methods (PSM, DSM, CBM, and RDBCM). The PDM had the best performance among the methods regarding the accuracy and the standard deviation of the estimates. A modified version of the PDM, the MPDM, was developed in order to encounter the presence of white noise in the data. The MPDM and the other four methods were tested on corrupted data with white noise for various values of signal to noise ratio (SNR). The MPDM and the PSM had the best performance even for low SNR. Finally, the PDM was applied for the classification of ultrasonic liver images, obtaining 95.2% right classification between normal and abnormal liver.

Future directions include the improvement of MPDM in order to encounter white noise of unknown variance and its extension for taking into account colored noise. Although the results of the classification between normal and abnormal liver were satisfactory, work must continue in order to distinguish different types of abnormalities.

TABLE 5
Estimation of the Fractal Dimension of the Ultrasonic Liver Images by the PDM

Normal		Hepatoma		Hemangioma	
Image	FD	Image	FD	Image	FD
N1	2.780	Hep1	2.984	Hem1	2.962
N2	2.898	Hep2	3.231	Hem2	3.454
N3	2.884	Hep3	3.071	Hem3	2.688
N4	2.739	Hep4	3.023	Hem4	3.092
N5	2.509	Hep5	3.152	Hem5	3.244
N6	2.499	Hep6	3.466	Hem6	2.909
N7	2.173	Hep7	3.285	Hem7	3.214
Mean	2.640		3.173		3.080
St.D.	0.262		0.169		0.252

ACKNOWLEDGMENT

The authors acknowledge the contribution of A. Nikita, M.D., of the Eugenidion Hospital, University of Athens, for providing and evaluating the ultrasonic liver images used in the study.

REFERENCES

1. B. B. Mandelbrot, *Fractal Geometry of Nature*, Freeman, San Francisco, 1982.
2. A. Pentland, Fractal-based description of natural scenes, *IEEE Trans. Pattern Anal. Mach. Intelligence* **6,** 1984, 661–674.
3. S. Peleg, J. Naor, R. Hartley, and D. Avnir, Multiple resolution texture analysis and classification, *IEEE Trans. Pattern Anal. Mach. Intelligence* **6,** 1984, 518–523.
4. T. Lundahl, W. J. Ohley, S. M. Kay, and R. Siffert, Fractional

Brownian motion: A maximum likelihood estimator and its applications to image texture, *IEEE Trans. Med. Imaging* **5,** 1986, 152–161.

5. L. M. Kaplan and C. C. J. Kuo, Texture roughness analysis and synthesis via extended self-similar (ESS) model, *IEEE Trans. Pattern Anal. Mach. Intelligence* **17,** 1995, 1043–1056.
6. J. M. Keller, S. Chen, and R. M. Crownover, Texture description and segmentation through fractal geometry, *Comput. Vision Graphics Image Process.* **48,** 1989, 150–166.
7. B. B. Chaudhuri and N. Sarkar, Texture segmentation using fractal dimension, *IEEE Trans. Pattern Anal. Mach. Intelligence* **17,** 1995, 72–77.
8. J. M. Keller and Y.-B. Seo, Local fractal geometric features for image segmentation, *Int. J. Imaging Systems Technol.* **2,** 1990, 267–284.
9. S. S. Chen, J. M. Keller, and R. M. Crownover, Shape from fractal geometry, *Artif. Intelligence* **43,** 1990, 199–218.
10. T. Peli, Multiscale fractal theory and object characterization, *J. Opt. Soc. Amer.* **7,** 1990, 1101–1112.
11. K. Arakawa and E. Krotkov, Fractal modelling of natural terrain: Analysis and surface reconstruction with range data, *Graph. Models Image Process.* **58,** 1996, 413–436.
12. G. W. Wornell and A. V. Oppenheim, Estimation of fractal signals from noisy measurements using wavelets, *IEEE Trans. Signal Process.* **40,** 1992, 611–623.
13. J. Samarabandu, R. Acharye, E. Hausmann, and K. Allen, Analysis of bone X-rays using morphological fractals, *IEEE Trans. Med. Imaging* **12,** 1993, 466–470.
14. R. L. Webber, T. E. Underhill, R. A. Horton, R. L. Dixon, and T. L. Pope Jr., Predicting osseous changes in ankle fractures, *IEEE Eng. Med. Biol.* **12,** 1993, 103–110.
15. C.-C. Chen, J. S. Daponte, and M. D. Fox, Fractal feature analysis and classification in medical imaging, *IEEE Trans. Med. Imaging* **8,** 1989, 133–142.
16. C. Fortin, R. Kumaresan, W. Ohley, and S. Hoefer, Fractal dimension in the analysis of medical images, *IEEE Eng. Med. Biol.* **11,** 1992, 65–71.
17. C. B. Coldwell, S. J. Stapleton, D. W. Holdsworth, R. A. Jong, W. J. Weiser, G. Cooke, and M. J. Yaffe, Characterisation of mammographic parenchymal pattern by fractal dimension, *Phys. Med. Biol.* **35,** 1990, 235–247.
18. B. B. Mandelbrot and J. W. van Ness, Fractional Brownian motion, fractional noise and applications, *SIAM Rev.* **10,** 1968, 422–437.
19. R. F. Voss, in *The Science of Fractal Images* (H.-O. Peitgen and D. Saupe, Eds.), Springer-Verlag, New York, 1988.
20. P. Flandrin, On the spectrum of fractional Brownian motion, *IEEE Trans. Inform. Theory* **35,** 1989, 197–199.
21. X. C. Jin, S. H. Ong, and Jayasooriah, A practical method for estimating fractal dimension, *Pattern Recognition Lett.* **16,** 1995, 457–464.
22. W. H. Press, S. A. Teukolsky, W. T. Vetterling, and B. P. Flannery, *Numerical Recipes in C: The Art of Scientific Computing,* Cambridge Univ. Press, Cambridge, UK, 1992.
23. N. Gache, P. Flandrin, and D. Garreau, Fractal dimension estimators for fractal Brownian motions, in *IEEE ICASSP-91*, pp. 3557–3560.
24. M. R. Rezaee, C. Nyqvist, P. M. J. Van der Zwet, E. Jansen, and J. H. C. Reiber, Segmentation of MR images by a fuzzy C-mean algorithm, *Comput. Cardiol.* 1995, 21–24.

PANTELIS ASVESTAS was born in Athens, Greece, on September 15, 1973. He received his diploma in electrical and computer engineering in 1996 from the National Technical University of Athens. He is awarded his Ph.D. from the National Technical University of Athens in nonlinear medical image processing using fractal theory. His interests include nonlinear image processing and optimization techniques applied to medical images. He is a member of the Technical Chamber of Greece.

GEORGE K. MATSOPOULOS received his diploma in electrical engineering in 1988 from the National Technical University of Athens. He received his M.Sc. in 1989 and his Ph.D. in bioengineering in 1993 from the University of Strathclyde. He is currently working as an assistant professor at the Institute of Communication and Computer Systems, National Technical University of Athens. His interests are nonlinear image processing applied to medical applications, 2-D and 3-D registration of medical images, and computer vision applications.

KONSTANTINA S. NIKITA received the diploma in electrical engineering and the Ph.D. from the National Technical University of Athens, Greece, in 1986 and 1990, respectively. She then received the M.D. from the University of Athens, Greece, in 1993. She is currently an assistant professor of the Department of Electrical and Computer Engineering, National Technical University of Athens. Her current research interests include applications of electromagnetic waves in medicine, clinical application of hyperthermia, electromagnetic scattering, diffraction tomography, nonlinear image processing, and optimization algorithms in medical applications. Dr. Nikita is a member of the Technical Chamber of Greece, the Medical Association of Athens, and the Hellenic Society of Biomedical Engineering.